JOURNAL OF MATERIALS SCIENCE 36 (2001) 2597–2605

Monte Carlo simulation of fatigue of a fibre tow undergoing chemical reaction

D. N. COON
University of Wyoming, Laramie, WY 82071, USA

A. M. CALOMINO
NASA - Glenn Research Centre, Cleveland, OH 44135, USA

Monte Carlo simulation has been used to model environmental attack of a fibre tow, and suggested that such attack could lead to fatigue-type behaviour under static load conditions. The system was assumed to be fibre dominated with the presence of matrix cracks relaxing stress in the matrix and providing a path for environmental species to reach the fibres. Lifetime under load was related to the fibre-environment reaction rate and distribution of forces from broken fibres. Fatigue exponents ranging from 1.0 to 1.5 were predicted for selected reaction rates at stress levels less than 140 MPa. Simulation results were compared with literature data, and predicted fatigue exponents were substantially lower than those observed experimentally. This result could suggest that fibre-environment chemical reaction was not the sole mechanism operable in experiments. However, it was suggested that a stress dependent reaction rate could be used to improve the correlation between the simulation and experimental results.

1. Introduction

Ceramic matrix composites are candidates for many high temperature structural applications. Lifetime at temperature under load is an important material characteristic for these applications. Limited lifetimes have been observed experimentally [1–12], and several degradation mechanisms have been identified including fibre-environment reaction, creep and wear of fibre surfaces during cyclic loading. Fibre-environment chemical reactions have been identified in high-temperature, oxidizing environments [13–15]. As a result, fibre coatings were developed to provide long lifetime (<10000 h) at elevated temperature (<1200 °C) [16–18]. Recently, lifetime degradation at intermediate temperatures (600–1000 °C) in composite systems containing coatings has been reported [6–10, 12].

Several researchers [7–10] have reported lifetimes as short as 2 h for enhanced SiC-SiC composites under constant load at temperatures below 1000 °C. These reduced lifetimes at intermediate temperatures are a significant concern for any application experiencing transient temperatures (heating and cooling cycles) under load [6]. One mechanism suggested for these short lifetimes was the reaction of fibres with environmental species at temperatures below which the coatings become effective [12]. Microstructural evidence of fibre damage in failed specimens consistent with a chemical reaction has been observed [19]. However, a relatively small fraction of the fibres in any given sample showed evidence of substantial reaction. Chemical reactions of SiC fibres with oxidizing environments have been reported [20–22], and the mechanism is generally related to oxidation of carbon fibre coatings. The presence of CO–CO_2 species in the environment has been shown to lead to chemical attack of SiC at temperatures as low as 700 °C [22–24].

The purpose of this communication is to simulate numerically a reaction between loaded fibres and oxidizing environments, and determine if the fatiguetype behaviour recently reported [7–9] could be expected to result form such a reaction mechanism.

2. Theoretical

2.1. Characteristics of Monte Carlo simulation of fibre reaction

Monte Carlo simulation is the numerical solution to physical problems containing probabilistic characteristics [25]. These probabilistic characteristics make analytical solutions difficult or impossible to develop. In Monte Carlo simulation, a computer performs calculations of system behaviour using mathematical relationships involving these probabilistic characteristics. In this manner, the solution is determined in part by the mathematical relationships, and, in part by the values of the various probabilistic characteristics. While any single solution will vary as the values of the probabilistic characteristics vary, performing the numerical solution many times can give insight into the behaviour of the physical system over the entire range of probabilistic characteristics. The validity of the numerical solution is determined by the appropriateness of the mathematical relationships and probabilistic characteristics. Random number generators, often called pseudo-random number generators, are used to determine the probabilistic characteristics. The effectiveness of the random number

generator in providing truly random numbers will determine the appropriateness of the probabilistic characteristics, and, therefore, the validity of the numerical solution.

The simulation described in this communication models a rectangular fibre tow that is loaded externally, exhibits mechanical behaviour that is fibre dominated, and undergoes a chemical reaction between exposed fibres and environmental species. The simulation allows only one fibre to react with the environment species initially, and the radius of the fibre reduces as a result of this reaction. The initial condition of a single reacting fibre is consistent with a matrix crack allowing environmental species access to some location in the fibre tow. As the radius of the reacting fibre decreases under a constant load, the stress on the reacting fibre increases. Eventually, the fibre breaks, and the load on the broken fibre is distributed to other fibres. Fibre failure was predicted using a critical strength approach by simply comparing fibre stress to fibre strength. Fibres neighbouring the broken fibre then begin to react as the access of the environmental species progresses through the fibre array. In this manner, the Monte carlo simulation iterates until complete failure of the fibre array occurs. A flow chart of the simulation is shown in Fig. 1.

The reaction between the fibres and environment was modelled as a gas–solid reaction that resulted in volatilization of fibre material. Reaction resulted in a reduction in the radius of any fibres exposed to the gaseous reactants, and the reaction was assumed to be a uniform surface reaction that removed an equal volume of fibre material in each iteration step. It was assumed that any deposition of volatilized species occurred in a manner that had no influence on subsequent reactions, i.e. the reaction rate never slowed due to diffusion through a product layer.

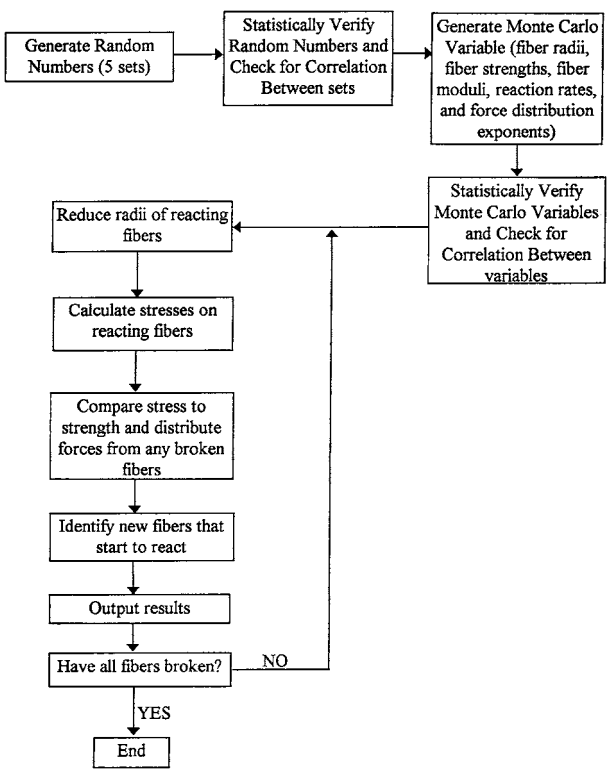

Figure 1 Flow chart of Monte Carlo simulation described in this communication.

External load could be transferred to individual fibres under either isostrain or isostress conditions. Isostrain conditions assume that individual fibres are in a uniform state of strain, but can be under differing states of stress. The stress in each individual fibre was calculated from the nominal stress, σ_{nom}, by assuming that the aggregate fibre stress, σ_{fibre}, could be calculated from

$$\sigma_{\text{fibre}} = \frac{\sigma_{\text{nom}}}{V_{\text{f}}} \tag{1}$$

where V_{f} is the volume fraction of the fibre.

An inherent assumption in Equation 1 is that all stress is transferred to fibres, and the matrix remains unstressed. This assumption is consistent with a fibre dominated system in which the matrix phase has fully cracked, and provides little mechanical integrity. The strain in the fibre array, σ_{fibre}, can be calculated using a simple uniaxial approximation

$$\varepsilon_{\text{fibre}} = \frac{\sigma_{\text{fibre}}}{E_{\text{fibre}}} \tag{2}$$

where E_{fibre} is the equivalent modulus of the fibre array.

Since the fibres are parallel to each other and perpendicular to the applied stress, the equivalent modulus of the fibre array can be calculated from [26]

$$E_{\text{fibre}} = \sum_i \sum_j \frac{E_{i,j}}{n} = \bar{E} \tag{3}$$

where $E_{i,j}$ is the modulus of fibre i, j; n is the number of fibres in the array; and $\bar{E}$ is the average fibre modulus.

Combining Equations 1–3, the strain in the fibre array was determined from

$$\varepsilon_{\text{fibre}} = \frac{\sigma_{\text{nom}}}{V_{\text{f}}\bar{E}} = \bar{\varepsilon}_{i,j} \tag{4}$$

where $\varepsilon_{i,j}$ is the strain in fibre i, j.

However, the strain in fibre i, j can also be expressed as

$$\varepsilon_{i,j} = \frac{\sigma_{i,j}}{E_{i,j}} \tag{5}$$

where $\sigma_{i,j}$ is the stress in fibre i, j; and $E_{i,j}$ is the modulus of fibre i, j.

Combining Equations 4 and 5, the stress in fibre i, j can be calculated from

$$\sigma_{i,j} = \left(\frac{\sigma_{\text{nom}}}{V_{\text{f}}}\right)\left(\frac{E_{i,j}}{\bar{E}}\right) \tag{6}$$

Notice that if the fibres all exhibit the same modulus, Equation 6 condenses to

$$\sigma_{i,j} = \left(\frac{\sigma_{\text{nom}}}{V_{\text{f}}}\right) = \sigma_{\text{fibre}} \tag{7}$$

Equation 7 suggests that all fibres would be under the same stress, and this condition corresponds to the isostress condition.

During the Monte Carlo simulation, the stress on each reacting fibre would be expected to increase in each iteration step as the radius decreases. The stress increase was modelled using a constant force assumption according to

$$(\sigma_{i,j})^{\text{new}} = (\sigma_{i,j})^{\text{prev}} \left[\frac{(r_{i,j})^{\text{prev}}}{(r_{i,j})^{\text{new}}} \right]^2 \quad (8)$$

Where $(\sigma_{i,j})^{\text{new}}$ is the stress on fibre i, j in the current iteration step; $(\sigma_{i,j})^{\text{prev}}$ is the stress on fibre i, j in the previous iteration step; $(r_{i,j})^{\text{prev}}$ is the radius of fibre i, j in the previous iteration step; and $(r_{i,j})^{\text{new}}$ is the radius of fibre i, j in the current iteration step.

The constant force assumption does not allow redistribution of forces in the fibre array until a fibre breaks. Therefore, a fibre that is not reacting will be under a state of constant stress until some other fibre breaks.

Distribution of force from a broken fibre to other fibres in the array was modelled as an inverse power law of the distance from the broken fibre according to

$$\Delta F_{i,j} = F_{\text{broken}} \left\{ \frac{1}{(d_{i,j})^n} \Big/ \sum_i \sum_j \left[\frac{1}{(d_{i,j})^n} \right] \right\} \quad (9)$$

where $\Delta F_{i,j}$ is the force distributed to fibre i, j; F_{broken} is the force from the broken fibre that is to be distributed to other fibres; $d_{i,j}$ is the distance from fibre i, j to the broken fibre; and n is the force disribution exponent.

Equation 9 can be summed over all fibres in the array to yield

$$\sum_i \sum_j \Delta F_{i,j} = \sum_i \sum_j F_{\text{broken}} \times \left\{ \frac{1}{(d_{i,j})^n} \Big/ \sum_i \sum_j \left[\frac{1}{(d_{i,j})^n} \right] \right\} = F_{\text{broken}} \quad (10)$$

and force balance in the fibre array is maintained as a fibre is broken and the force on that fibre is distributed to remaining fibres.

2.2. Development and verification of Monte Carlo variables

Monte Carlo variables developed by the simulation included

- fibre radii;
- fibre strength;
- fibre moduli;
- reaction rates of individual fibres with the environment;
- force distribution exponents of individual fibres.

The physical and mechanical characteristics of Nicalon^{TM} fibres have been extensively studied [27–33]. The fibre radii were modelled as a Gaussian distribution about a mean of 6.9 μm and a standard deviation of 1.3 μm [33]. The fibre strengths were modelled as a Weibull distribution with a characteristic strength of 1.1 GPa and Weibull parameter of 3.6 [28]. The fibre moduli were modelled as Gaussian distribution about an average of 145 GPa and a standard deviation of 60 GPa [28]. The fibre reaction rates were modelled as a uniform distribution $\pm 10\%$ from the expected value (the reaction rate of individual fibres was randomly distributed from 90 to 110% of the expected value). The force distribution exponents were modelled as a uniform distribution ± 1 from the expected value (the force distribution exponent of individual fibres was randomly distributed from $n - 1$ to $n + 1$).

Since the effectiveness of the random number generator determines the validity of the numerical results in any Monte Carlo simulation, great care must be taken to ensure that the random number generator is well behaved. The random number generator used in this simulation was based on the method of L'Ecuyer with the addition of a Bays–Durham shuffle [34]. Five independent sets of random numbers were used to generate fibre radii, fibre strengths, fibre moduli, fibre reaction rates, and force distribution exponents, respectively. The effectiveness of each set of random numbers generated was checked using both chi-square and Kolmogorov–Smirnov goodness-of-fit tests. The chi-square goodness-of-fit [35] test compares the shape of the random number distribution in the form of a discrete distribution with the expected shape of a uniform distribution. The Kolmogorov–Smirnov goodness-of-fit [36] test compares the shape of the random number distribution in the form of a continuous distribution with the expected shape of a uniform distribution. While other statistical tests have been proposed [35], the chi-square- and Kolmogorov–Smirnov tests are the most common. Failure of either the chi-square or Kolmogorov–Smirnov tests was defined to be greater than or equal to 5% probability that the generated numbers were not random.

The fibre radii generated were compared with a Gaussian distribution exhibiting the expected mean and standard deviation with a chi-square goodness-of-fit test. Fibre strengths generated were compared with the expected Weibull distribution using a chi-square goodness-of-fit test. Fibre Moduli generated were compared with the expected Gaussian distribution using a chi-square goodness-of-fit test. In each case, failure of these chi-square tests was defined as a greater than or equal to 5% probability that the Monte Carlo variables were not consistent with the respective distributions.

Fibre radii are expected to be determined primarily by processing method, fibre strengths are expected to be determined primarily by handling damage (flaws), and fibre moduli are expected to be determined primarily by chemical and microstructural characteristics. As a result, correlation of random number sets and Monte Carlo variables developed from those random number sets was a concern. In particular, correlation of radii and strengths, radii and moduli, and strengths and moduli was thought to be inappropriate. Random numbers were checked using the Pearson correlation test in pairs to examine correlation between the random numbers used to generate (i) fibre radii and strengths, (ii) fibre radii and

moduli, and (iii) fibre strengths and moduli. In addition, Monte Carlo variables derived from the random numbers were checked in pairs for correlation of (i) radii and strengths, (ii) radii and moduli, and (iii) strengths and moduli. In each case, failure of each correlation test was defined as a greater than or equal to 5% probability that the pair was correlated.

The generation of random numbers or development of Monte Carlo variables from those numbers was considered valid only if all of the above tests were passed. Two exceptions were in the chi-square and Kolmogorov–Smirnov goodness-of-fit tests of the random number sets used to generate the fibre radii and moduli. The polar transformation method [37] was used to generate radii and moduli within Gaussian distributions from these random numbers. As a result of the polar transformation, the random numbers may not pass standard goodness-of-fit tests. However, this result is of little concern if the radii and moduli do pass goodness-of-fit tests when compared with expected Gaussian distributions. Other than the two exceptions, failure of any statistical resulted in the simulation results being discarded, and the simulation rerun. Simulations were run at least ten times with any set of input variables, and the system behaviour was then reported as the average and the error was reported as three times the standard error of the mean [36]. In this way, the results (average $\pm$ error) should encompass more than 99% of the possible averages of ten simulation runs with a given set of input variables.

3. Results

Important input variables were the nominal applied stress, the volume fraction of fibre, the size (length and width) of the fibre array, and the fibre initially undergoing reaction (reaction origin). The value of nominal stress was varied from 5 to 20% of the fibre strength. The volume fraction of fibre was held constant at 40%. Using these two characteristics, aggregate fibre stress (Equation 1) varied from 12.5 to 50% of the fibre strength. The size of the fibre array was held constant at 41 fibres long and 12 fibres wide (492 total fibres in a tow) [19]. Four possible reaction origins were considered. The reaction origin identified as corner, was defined as the fibre initially undergoing reaction situated in the upper right-hand corner of the fibre array. The reaction origin identified as centre, was defined as the fibre initially undergoing reaction situated in the geometric centre of the fibre array. The reaction origin identified as centred on the long edge was identified as the fibre initially undergoing reaction centred on the left-hand edge of the fibre array. The reaction origin indentified as centred on the long edge was indentified as the fibre initially undergoing reaction centred on the upper edge of the fibre array. Three of the reaction origins (corner, centred on short edge, and centred on long edge) have obvious physical significance associated with the likely path of reactants from the environment to the fibre tow. The fourth reaction origin (centre) has little physical significance, but resulted in some interesting numerical correlations with the other three reaction origins.

Typical simulation results are shown in Fig. 2. Even though the nominal stress was only 10% of the characteristic fibre strength, the fibre array in the initial state (Fig. 2a) contains about 1.6% broken fibres. These broken fibres are the low strength fibres predicted from a low Weibull parameter (wide strength distribution). The origin of the fibre–environment reaction, is the fibre in the upper left corner of the array. Fig. 2b shows the fibre array after approximately 5% of the fibres have broken. A region of fibre failure developed radially from the origin of the reaction. All of the fibres in this region have under gone some chemical reaction with environmental species. In addition, one fibre broke from pure mechanical loading without any chemical reaction with the environment. Fig. 2c shows the fibre array after approximately 10% of the fibres have broken. Failure is clearly proceeding by growth of the region undergoing chemical reaction with the environment. However, it appears that growth is occurring preferentially along the short edge of the fibre array. Fig. 2d shows the fibre array after approximately 20% of the fibres have broken. Notice the region of fibre failure has now grown completely across the short edge of the fibre array. Also, a few other fibres have broken from pure mechanical loading without the presence of a fibre–environment chemical reaction. In Fig. 2e (approximately 35% of the fibres broken) the region of fibre failure has begun growing across the long dimension of the fibre array. In Fig. 2f (approximately 50% of the fibres broken) the region of fibre failure accounted for the left half of the fibre array.

Fig. 2 shows some important characteristics of the simulation results. First, some fibres break on initial loading due the wide strength distribution, but the percentage of fibres broken on initial loading is typically less than 2%. Second, the region of broken fibres tends to grow across the short dimension of the fibre array before appreciable growth across the long dimension occurs. The growth across the short dimension of the array corresponds to 15–20% of the fibres breaking. This growth characteristic is largely independent of the origin of the chemical reaction. Third, reaction of fibre with environmental species dominates fibre failure during most of the lifetime. Some fibres that are not undergoing chemical reaction break (pure mechanical failure), but account for few fibre failures until late in the stimulation.

Fig. 3 shows the percent broken fibres as a function of the time step (time in the simulation) for ten simulations where the reaction origin was the upper left corner and ten simulations where the reaction origin was the centre of the fibre array. Two characteristics are largely independent of reaction origin. First, the per cent of fibres broken is highly non-linear with time step, and the general shape is independent of reaction origin. Little increase in the per cent of broken fibres occurs in the first 75% of the lifetime, and the majority of the increase in the percent of broken fibres occurs in the last 25% of the lifetime. The change in rate of increase of percent fibres broken corresponds reasonably well with the change in growth pattern form growth primarily along the short dimension of the array (<15–20%

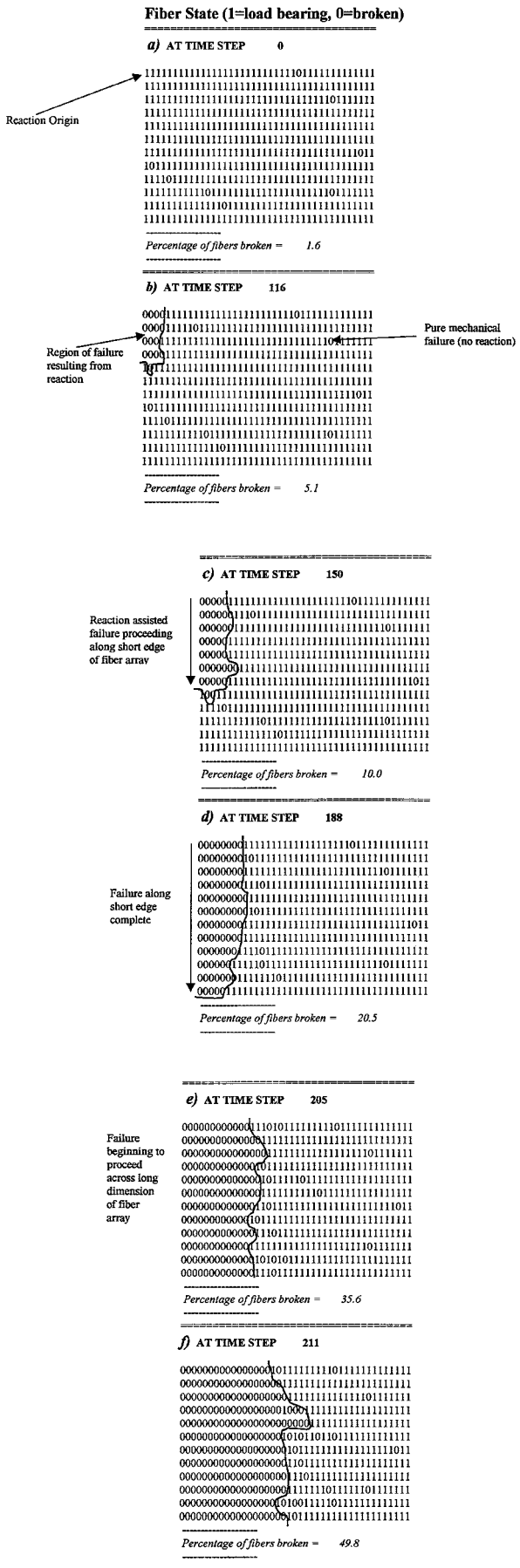

Figure 2 Fibre array showing both load bearing (represented by 1) and broken (represented by 0) fibres at (a) time step 0, (b) time step 116, (c) time step 150, (d) time step 188, (e) time step 205, and (f) time step 211. The simulation parameters were isostrain conditions, a nominal stress of 10% of the characteristic fibre stress, 40% by volume fibre, an expected force distribution exponent of two, an expected reaction rate of 1% per time step, and a reaction origin at the upper left corner.

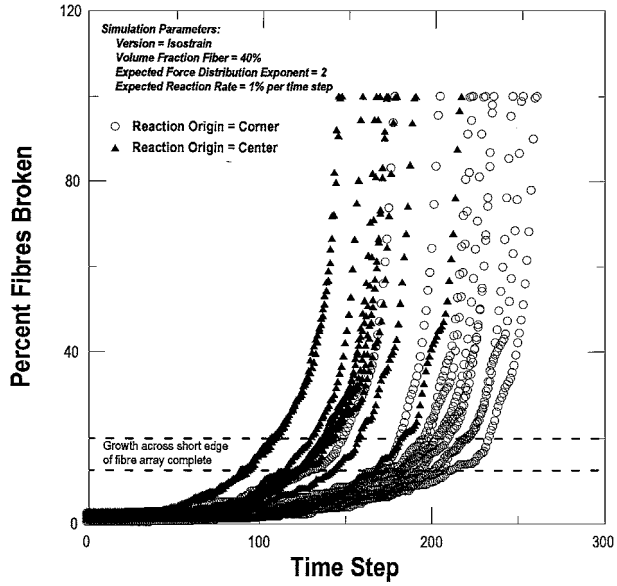

Figure 3 Percent broken fibres as a function of simulated time for a reaction origin in the corner (ten simulations) and a reaction origin in the centre (ten simulations): ○, reaction origin = corner; ▲, reaction origin = centre.

fibres broken) to growth primarily along the long dimension of the array (>20% fibres broken). Second, reaction origins in the corner of the array tend to yield longer lifetimes than reaction origins in the centre.

The trend that the majority of the lifetime corresponds to a region where less than 15–20% of the fibres have failed would suggest that a relatively small fraction of the fibres in the array would show appreciable radius reductions at the conclusion of the simulation. The result is consistent with microstructural evidence of fibre-environmental reaction in failed SiC–SiC composites [19].

Fig. 4 shows the effect of the force distribution exponent (n in Equations 9 and 10) on the lifetime for reaction origins in the upper left corner, in the geometric

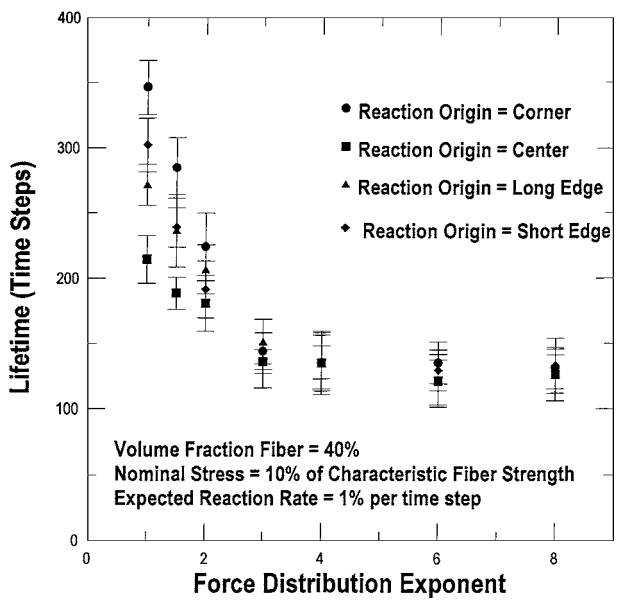

Figure 4 Predicted lifetime as a function of force distribution exponent and reaction origin: ●, reaction origin = corner; ■, reaction origin = centre; ▲, reaction origin = long edge; ♦, reaction origin = short edge.

centre, centred on the upper long edge, and centred on the left short edge of the fibre array. For force distribution exponents of three or larger, the lifetime was independent of reaction origin or force distribution exponent. However, for force distribution exponents between one and two, the lifetime increased as the force distribution exponent decreased. If the force distribution exponent is controlled primarily by the fibre-matrix interface characteristics, this result supports the concept that interface design is vital to composite behaviour. In addition, the longest average lifetime was calculated for a reaction origin at the corner, and the shortest average lifetime was calculated for a reaction origin at the centre. Reaction origins centred on the long or short edge of the array yielded intermediate results. From Fig. 4, the reaction origin had a significant influence on the predicted lifetime at low force distribution exponents.

The effect of the force distribution exponent is to localize the distribution of forces from broken fibres (Equation 9). As the force distribution exponent increases, the fibres neighbouring broken fibres receive a larger fraction of the force distributed from those broken fibres. Fig. 5 shows the effect of the normalizing term (denominator in Equation 9) on the predicted lifetime for reaction origins in the upper left corner, geometric centre, centred on the long edge, and centred on the short edge. As the force distribution exponent increases, the denominator in Equation 9 decreases. Fig. 5 clearly shows a non-linear decrease in lifetime with decrease in the normalizing term. The normalizing term for force distribution exponents of four, six and eight is largely independent of reaction origin, and the lifetimes are largely independent of reaction origin. This trend suggests that near-neighbour effects dominate at force distribution exponents greater than four.

The dashed lines in Fig. 5 are lines of constant force distribution exponents for exponents less than three. In these cases, the lifetimes decrease as the reaction origin changes from the corner to the centre even though the normalizing term increases. Reaction origins centred on the long and short edge of the fibre array yield intermediate results. This trend suggests that near-neighbour effects play a secondary role for force distribution exponents less than two. Remember that two stages of fibre failure are evident in Fig. 3. The initial stage (low rate of increase of percent of fibres broken) occurs with progression of the region of fibre failure across the short dimension of the array. The second stage (high rate of increase of percent of fibres broken) occurs when the region of fibre failure grows across the long dimension of the array. For a reaction origin in the upper left corner (Fig. 6a), the region of fibre failure must grow across the entire width of the array before the initial stage is completed. Completion of the second stage requires growth across the entire array length. For a reaction origin in the centre of the array (Fig. 6b), the region of fibre failure must grow across one-half the width of the array in the initial stage, and one-half the length of the array in the second stage. It should be noted that growth occurs from the reaction origin in opposite directions simultaneously in both the initial and second stages. A reaction origin centred on the short edge (Fig. 6c), the region of fibre failure must grow across one-half the width of the array in the initial stage, and across the entire length in the second stage. For a reaction origin centred on the long edge (Fig. 6d), the region of fibre failure must grow across the entire width of the array in the initial stage, and across one-half the length in the second stage.

If the rate of growth of the region of fibre failure is assumed to be independent of reaction origin, the lifetime should correlate to a combination of the distances

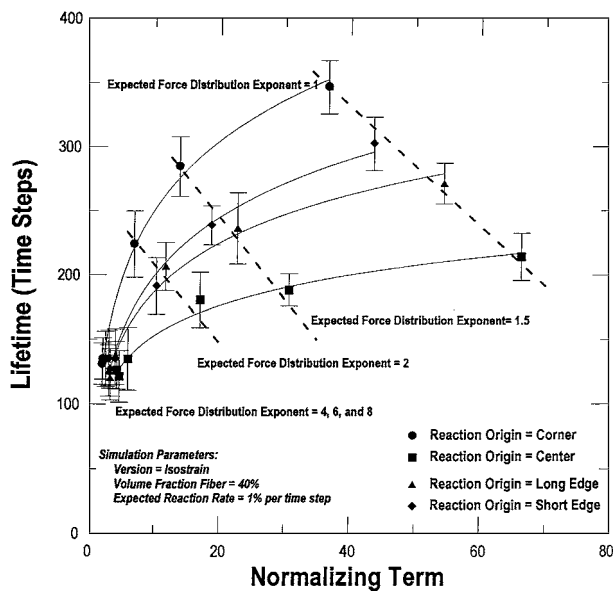

Figure 5 Predicted lifetime as a function of the normalizing term in Equation 9 and reaction origin. The dashed lines are lines of constant force distribution exponent: ●, reaction origin = corner; ■, reaction origin = centre; ▲, reaction origin = long edge; ♦, reaction origin = short edge.

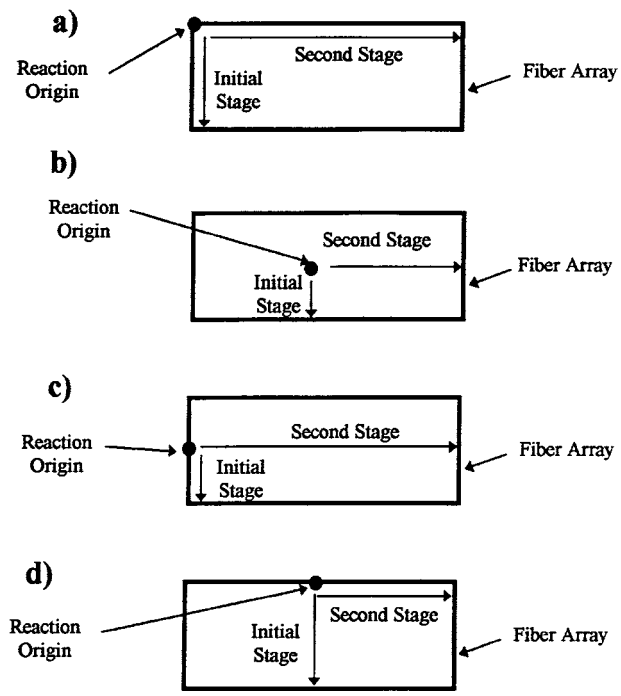

Figure 6 Schematic of the direction of growth of the region of fibre failure for both the initial and second stages for (a) reaction origin in the upper left corner, (b) reaction origin in the geometric centre, (c) reaction origin centred on the short edge, and (d) reaction origin centred on the long edge.

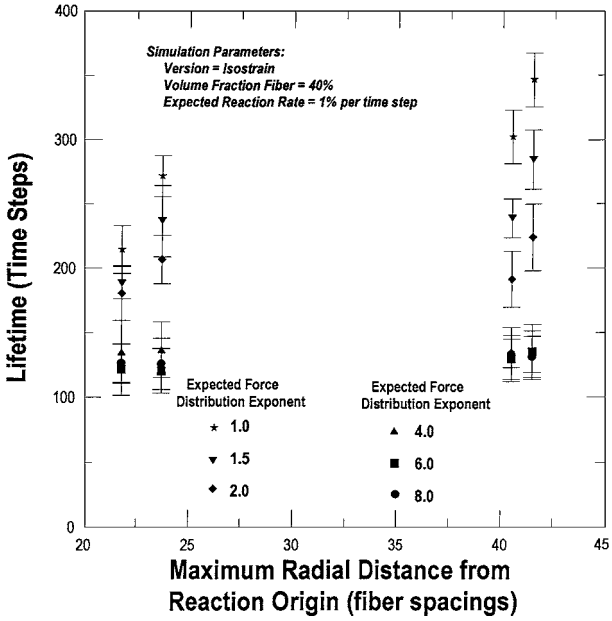

Figure 7 Predicted lifetime as a function of the maximum radial distance from the reaction origin to the farthest corner of the fibre array.

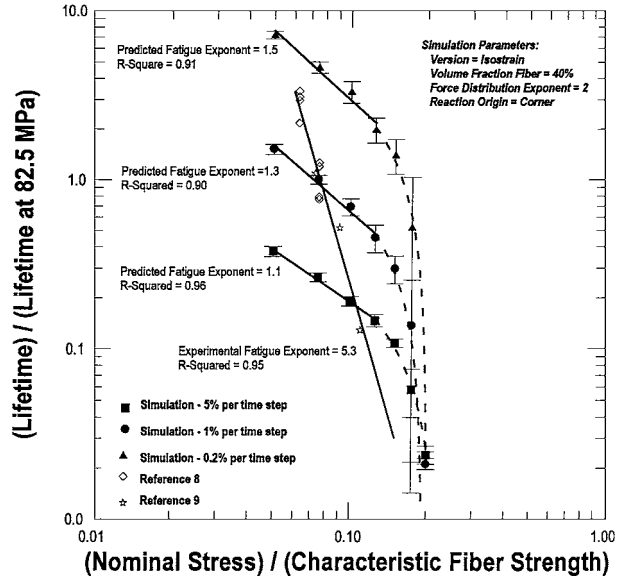

Figure 8 Normalized lifetime as a function of normalized nominal stress.

of growth in both the initial and second stages. An appropriate combination of these distances would be the maximum radial distance from the reaction origin to the furthest corner of the array $d_{\max}$ given by

$$d_{\max} = \left[(d_{\text{initial}})^2 + (d_{\text{second}})^2\right]^{1/2} \tag{10}$$

where d_{initial} is the distance of growth in the initial stage and d_{second} is the distance of growth in the second stage.

Fig. 7 shows the lifetime as a function of maximum radial distance, $d_{\max}$ Fig. 7 does show a trend of increased lifetime for increased maximum radial distance for force distribution exponents of 1, 1.5 and 2.0. At the same time, the lifetime is independent of the maximum radial distance for force distribution exponents of four, six and eight. Also apparent is the trend that a reduction of force distribution exponent has a more pronounced influence on the lifetime for reaction origin characterized by larger maximum radial distances. Therefore, a change of force distribution exponent from four to one caused a more dramatic increase in lifetime for a reaction origin at the corner ($d_{\max} = 41.5$ fibre spacings) than for a reaction origin at the geometric centre ($d_{\max} = 21.8$ fibre spacings).

Fatigue type behaviour is traditionally [38] quantified by the following expression

$$t_{\text{f}} = A(\sigma_{\text{nom}})^{-n_{\text{f}}} \tag{11}$$

where t_{f} is the lifetime; A, a constant; σ_{nom}, the nominal stress; and n_{f} the fatigue exponent.

Equation 11 can be written in normalized form as follows

$$\frac{t_{\text{f}}}{(t_{\text{f}})^{82.5\,\text{MPa}}} = \left\{\left[\frac{(\sigma_{\text{char}})^{-n_{\text{f}}}}{(t_{\text{f}})^{82.5\,\text{MPa}}}\right]A\right\}\left(\frac{\sigma_{\text{nom}}}{\sigma_{\text{char}}}\right)^{-n_{\text{f}}} \tag{12}$$

where $(t_{\text{f}})^{82.5\,\text{MPa}}$ is the lifetime at 82.5 MPa, and σ_{char} is the characteristic fibre strength.

Normalizing to the lifetime at 82.5 MPa applied stress permitted convenient comparison of the numerical results with experimental results reported in the literature. Fig. 8 shows the effect of stress on lifetime plotted according to Equation 12. Simulation results predicted from expected reaction rate of 5, 1 and 0.2% per time step are shown in Fig. 8. The simulation results have been normalized to the average lifetime at 82.5 MPa and an expected reaction rate of 1% per time step predicted by the simulation. Clearly, the lifetime decreased as the stress increases. Between normalized stress levels of 0.05 and 0.125 (solid lines in Fig. 8) behaviour consistent with Equation 12 was observed. Fatique exponents of 1.5, 1.3 and 1.1 were calculated for simulation results predicted from expected reaction rates of 0.2, 1 and 5% per time step, respectively. This behaviour is consistent with fatiguetype behaviour. It should be noted that at normalized stress levels below 0.05 (about 50 MPa nominal stress), no matrix crack formation has been reported [39], and the environment would not have a path to the fibres. For normalized stress levels greater than 0.125, the simulation results did not follow a trend consistent with Equation 12. At high stress levels (normalized stress of 0.20), the lifetimes converged to a constant independent of expected reaction rate. This result suggested the simulation was dominated by stress at high stress levels.

Also shown in Fig. 8 is the data of Verrilli *et al.* [8] at nominal stress levels of 69 and 82.5 MPa and temperatures ranging from 600 to 982 °C and the data of Lara-Curizo [9] at stress levels of 80, 100 and 120 MPa at a temperature of 950 °C. The experimental data have been normalized to experimental data at 82.5 MPa [8]. The experimental data clearly show a decreased lifetime with increased nominal stress, but show a more rapid change in lifetime with changes in stress. Also, the experimental data clearly show more variability at any stress than predicted by the simulation. It is not possible to draw a direct correlation between the simulation and reported experimental results since the rate

of carbon oxidation was studied [9], but the rate of fibre attack was not reported [8, 9]. In addition, the experimental data were developed using composites characterized by stacked layers with each layer characterized by a 0–90° plain weave.

While the simulation suggests that the fatigue exponent increases with decreased reaction rates, a very slow reaction rate may show excellent correlation to the experimental data. However, such a correlation would require sufficient knowledge of the fibre–environment reaction process to yield a correlation between real time (hours) and simulated time (time steps). However, since the experimental data appear to cross the simulation results in such a way as to suggest a functional dependence between the nominal stress and reaction rate, an alternate approach to simulating the experimental data could be used. Using the results in Fig. 8 as a calibration, the following empirical model was developed

$$R = (0.0078)\exp(0.406)\sigma_{\text{nom}} \qquad (13)$$

where R is the expected reaction rate.

An exponential dependence of reaction rate on stress has been suggested as an explanation of fatigue crack growth in monolithic ceramics [40]. Fig. 9 shows the results of the simulation using Equation 13 to determine the expected reaction rate as a function of nominal stress and experimental data of Verrilli *et al.* [8] and Lara-Curzio [9]. The simulation shows excellent correlation with the experimental data. However, since Equation 13 was based on an empirical fit of the experimental data, the excellent correlation does not prove that the experimental data result from a reaction mechanism. However, the Monte Carlo simulation modelling fibre-environment reactions do suggest fatigue-like behaviour. At the same time, the numerical results could be interpreted as suggesting that mechanisms other than reaction of fibres with environmental species dominated the experimental results reported in the literature.

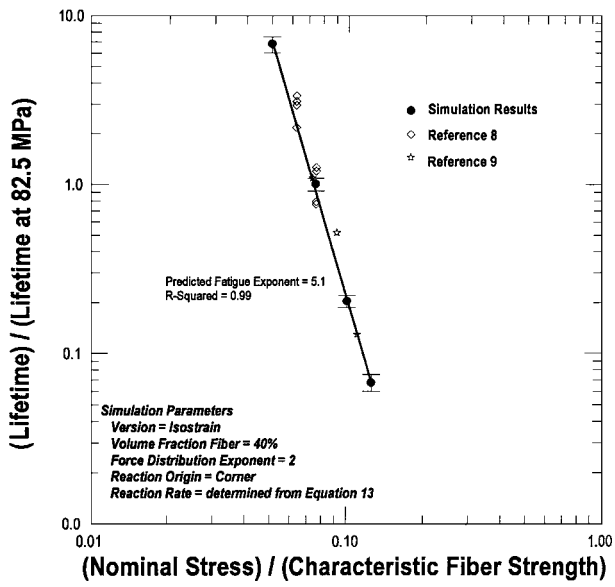

Figure 9 Comparison of predicted normalized lifetimes based on reaction rates determined by nominal stress as a function of normalized nominal stress with literature values.

4. Conclusions

A Monte Carlo simulation examining the effect of fibre–environment reaction and static mechanical load on the behaviour of a fibre tow has been developed. Fibres were allowed to react with environmental species only when an identifiable path for the reactants existed, and forces were distributed using an inverse power law as the fibre broke. At force distribution exponents greater than about three, the lifetime was independent of origin of the fibre–environment reaction. However, at force distribution exponents less than about two, the origin of the fibre–environment reaction did affect the lifetime. Simulation results were shown to be dependent on the magnitude of the mechanical load and the rate of fibre–environment reaction. Fatigue exponents ranging from about 1.0 to 1.5 were predicted for nominal stress levels less than 140 MPa and reaction rates ranging from 5% per time step to 0.2% per time step, respectively. Comparison of simulation results with literature values suggested that the simulation underestimated the observed fatigue exponent. It was shown that a reaction rate dependent on the nominal stress level could be used to simulate literature results empirically. Further investigation of fibre–environment reaction rates at intermediate temperatures is required before a definitive relationship can be developed.

References

1. L. X. HAN and S. SURESH, *J. Amer. Ceram. Soc.* **72** (1989) 1233.
2. J. W. HOLMES, *ibid.* **74** (1991) 1639.
3. L. P. ZAWADA, L. M. BUTKUS and G. A. HARTMAN, *ibid.* **74** (1991) 2851.
4. S. F. SHULER, J. W. HOMES, S. WU and D. ROACH, *ibid.* **76** (1993) 2327.
5. S. RAGHURAMAN, J. F. STUBBINS, M. K. FERBER and A. A. WERESZCZAK, *J. Nuclear Mater.* **212–215** (1994) 840.
6. D. W. WORTHEM, NASA Lewis Research Center, Report No. 195441 March (1995).
7. M. H. HEADINGER, P. E. GRAY and D. H. ROACH, Paper presented at the Composites and Advanced Structures Cocoa Beach Conference, January (1995).
8. M. J. VERRILLI, A. M. CALOMINO and D. N. BREWER, Paper presented at the Composites and Advanced Structure Cocoa Beach Conference, January (1996).
9. E. LARA-CURZIO, "Stress Rupture of Nicalon™/SiC CFCC's" (Oak Ridge National Laboratory, 1996).
10. H. T. LIN, P. F. BECHER, K. L. MORE, P. F. TORTORELLI and E. LARA-CURZIO, "Evaluation of Stress-Temperature-Lifetime Working Envelop for Enhanced Nicalon-SiC CFCC's" (Oak Ridge National Laboratory, 1996).
11. M. MIXUNO, S. ZHU, Y. NAGANO, Y. SAKAIDA, Y. KAGAWA and M. WATANABE, *J. Amer. Ceram. Soc.* **79** (1996) 3065.
12. E. Y. SUN, S. T. LIN and J. J. BRENNAN, *ibid.* **80** (1997) 609.
13. J. J. BRENNAN, "Materials Science Research," Vol. 20 (Plenum Press, New York, 1986) p. 549.
14. R. F. COOPER and K. CHYUNG, *J. Mater. Sci.* **22** (1987) 3148.
15. H. C. CAO, E. BISCHOFF, O. SBAIZERO, M. RUHLE, A. G. EVANS, D. B. MARSHALL and J. J. BRENNAN, *J. Amer. Ceram. Soc.* **73** (1989) 1691.
16. R. W. RICE, US Patent No. 4642271, February (1987).
17. *J. Amer. Ceram. Soc.* **72** (1989) 1764.
18. R. NASLAIN, O. DUGNE and A. GUETTE, *ibid.* **74** (1991) 2482.
19. A. M. CALOMINO, Private communication.
20. R. T. BHATT, *J. Amer. Ceram. Soc.* **75** (1992) 405.

21. K. P. PLUCKNETT and M. H. LEWIS, *J. Mater. Sci. Lett.* **14** (1995) 1223.
22. L. FILIPUZZI, G. CAMUS and R. NASLAIN, *J. Amer. Ceram. Soc.* **77** (1994) 449.
23. D. BUTT, R. E. TRESSLER and K. SPEAR, *ibid.* **75** (1992) 3257.
24. S. M. JOHNSON, R. D. BRITTAIN, R. LAMOREAUS and D. J. ROWECLIFFE, *ibid.* **71** (1988) C132.
25. T. NARUSHIMA, T. GOTO, Y. YOKOYAMA, M. TAKEUCHI, Y. IGUCHI and T. HIRAI, *ibid.* **77** (1994) 1079.
26. W. D. CALLISTER, JR, "Materials Science and Engineering—An Introduction" (Wiley, New York, 1997) p. 513.
27. R. S. ZIMMERMAN and D. F. ADAMS, NASA, Report No. 177 525 (1989).
28. G. SIMON and A. R. BUNSELL, *J. Mater. Sci.* **19** (1984) 3649.
29. L. C. SAWYER, M. JAMIESON, D. BRIKOWSKI, M. I. HAIDER and R. T. CHEN, *J. Amer. Ceram. Soc.* **70** (1987) 798.
30. D. J. PYSHER, K. C. GORETTA, R. S. HODDER, JR. and R. E. TRESSLER, *ibid.* **72** (1989) 284.
31. A. J. ECKEL and R. C. BRADT, *ibid.* **72** (1989) 455.
32. F. W. ZOK, X. CHEN and C. H. WEBER, *ibid.* **78** (1995) 1965.
33. A. M. CALOMINO, Private communication.
34. W. H. PRESS, S. A. TEUKOLSKY, W. T. VETTERLING and B. P. FLANNERY, "Numerical Recipes in Fortran. The Art of Scientific Computing," 2nd edn (Cambridge, University Press, Cambridge, 1992).
35. E. J. DUDEWICZ and T. G. RALLEY, "The Handbook of Random Number Generation and Testing with TESTRAND Computer Code" (American Sciences Press, Inc., Columbus, OH, 1981).
36. R. V. HOGG and E. A. TANIS, "Probability and Statistical Inference" (Macmillan, New York, 1983).
37. D. E. KNUTH, "The Art of Computer Programming," 2nd edn (Addison Wesley, 1981).
38. R. W. DAVIDGE, "Mechanical Behavior of Ceramics" (Cambridge University press, Cambridge, 1979) p. 144.
39. S. M. SPEARING, F. W. ZOK and A. G. EVANS, *J. Amer. Ceram. Soc.* **77** (1994) 2381.
40. S. M. WEIDERHORN, *ibid.* **55** (1972) 81.
41. R. Y. RUBINSTEIN, "Simulation and the Monte Carlo Method" (Wiley, New York, 1981).

Received 28 January
and accepted 16 June 1998